Chemistry Faculty Research & Creative Works   Chemistry

01 Oct 2019

State-To-State Inelastic Rotational Cross Sections in Five-Atom Systems with the Multiconfiguration Time Dependent Hartree Method

Steve Ndengue

Yohann Scribano

Fabien Gatti

Richard Dawes
Missouri University of Science and Technology, dawesr@mst.edu

State-to-state inelastic rotational cross sections in five-atom systems with the multiconfiguration time dependent Hartree method

View Online · Export Citation · CrossMark

Steve Ndengué,[1,2] (iD) Yohann Scribano,[3] (iD) Fabien Gatti,[4] and Richard Dawes[2,a] (iD)

AFFILIATIONS

[1] ICTP-East African Institute for Fundamental Research, University of Rwanda, Kigali, Rwanda
[2] Department of Chemistry, Missouri University of Science and Technology, Rolla, Missouri 65409, USA
[3] Laboratoire Univers et Particule de Montpellier, Université de Montpellier, UMR-CNRS 5299, 34095 Montpellier Cedex, France
[4] Institut de Sciences Moléculaires d'Orsay, UMR 8214, Université Paris-Sud - Université Paris-Saclay, 91405 Orsay, France

[a] dawesr@mst.edu

ABSTRACT

We present a MultiConfiguration Time Dependent Hartree (MCTDH) method as an attractive alternative approach to the usual quantum close-coupling method that approaches some computational limits in the calculation of rotational excitation (and de-excitation) between polyatomic molecules (here collisions between triatomic and diatomic rigid molecules). We have performed a computational investigation of the rotational (de-)excitation of the benchmark rigid rotor H_2O–H_2 system on a recently developed Potential Energy Surface of the complex using the MCTDH method. We focus here on excitations and de-excitations from the 0_{00}, 1_{11}, and 1_{10} states of H_2O with H_2 in its ground rotational state, looking at all the potential transitions in the energy range 1–200 cm^{-1}. This work follows a recently completed study on the H_2O–H_2 cluster where we characterized its spectroscopy and more generally serves a broader goal to describe inelastic collision processes of high dimensional systems using the MCTDH method. We find that the cross sections obtained from the MCTDH calculations are in excellent agreement with time independent calculations from previous studies but does become challenging for the lower kinetic energy range of the de-excitation process: that is, below approximately 20 cm^{-1} of collision energy, calculations with a relative modest basis become unreliable. The MCTDH method therefore appears to be a useful complement to standard approaches to study inelastic collision for various collision partners, even at low energy, though performing better for rotational excitation than for de-excitation.

Published under license by AIP Publishing. https://doi.org/10.1063/1.5119381

I. INTRODUCTION

Our understanding of energy transfer between colliding atoms and molecules is crucial for several fields such as chemical processes in the Earth's atmosphere, combustion chemistry processes for industrial and aeronautic applications, and also outside Earth's environment, such as in the InterStellar Medium (ISM), and stellar and planetary (and exoplanetary) atmospheres.[1–4] For example, determination of molecular abundances in protostellar clouds requires one to solve radiative transfer equations, which themselves require knowledge of state-to-state rotational excitation (and de-excitation) rate constants. The most accurate technique to determine accurate rotational inelastic cross sections (and thus rate constants)

is certainly the time independent quantum method based on Close Coupling (CC) that solves the nuclear Schrödinger equation. The CC methodology is a powerful and intuitive method to solve for the rovibrational states and obtain the collisional cross sections using a potential energy function typically obtained by means of accurate *ab initio* methods. This approach was intensively used in the past for the simulation of rotationally inelastic collisions of nonreactive diatomic and polyatomic molecules with atoms and molecular colliders such as H_2, which is the most abundant molecule in space. The other well-known technique is the quasiclassical trajectory method, which solves the classical Hamilton's equations of motion, and is usually processed by quantizing the classical action of trajectories using binning histogram methods. This approach is

numerically very efficient since computational time decreases as the collision energy increases. However, the QCT approach is best suited for the high temperature regime where quantum effects are expected to be less important, whereas for low temperature, its validity could be questionable. More recently, the mixed quantum-classical trajectory (MQCT)[5] and statistical adiabatic channel model (SACM)[6,7] have been proposed as alternative approaches to the CC method and they both have shown very promising results in certain cases, but less accurate behavior in other cases, with their domain of validity not yet fully known and needing to be investigated.

In this work, we want to address another alternative approach that can have some numerical advantages compared to CC approaches and especially when we consider high-dimensional molecular systems for which the density of internal rovibrational states is large leading to unfeasible CC simulations. Here, we extend a recently reported MCTDH investigation[8] of Ar colliding with a rigid triatomic rotor (H_2O) by studying the collision between diatomic rigid rotors with triatomic rigid rotors using the MCTDH methodology. This five-dimensional system corresponds to the description of rigid rotors inelastic rotational excitation, an example of which is H_2O colliding with H_2, a system of interest for ISM and astrochemistry. In the past, the spectroscopy of the weakly bounded complex H_2O–H_2 was intensively studied[9–13] but also the collisional dynamics between those two molecules with various methods. Those methods used Time Independent CC formalism,[11,14–20] as well as quasiclassical approach,[21] which makes this system a very good five-dimensional benchmark. The MCTDH method has emerged in recent years as one of the methods of choice for the study of the quantum molecular dynamics (spectroscopy or collisional dynamics) for the system in high dimensionality. We are particularly focused here on the low-energy collision region in order to most stringently test the method. This is because of the resonance structures mentioned before, and also because of the known difficulty for time-dependent approaches to describe low-energy collisions, since the wavepacket in that case moves slowly, and the propagation then takes a very long time (which may lead to a propagation of errors).

This paper is organized as follows: in Sec. II, we will first give a brief introduction to the MCTDH method and the Hamiltonian [the kinetic energy operator (KEO) and the potential energy surfaces (PES)] used for the dynamics, and in Sec. II D, we will describe how the cross sections are obtained and discuss the convergence of the calculations. In Sec. III, we will present our results and their comparison to CC simulations. We will finally conclude in Sec. IV and give some perspectives of this method for more complex molecular systems.

II. COMPUTATIONAL METHODOLOGY

A. MCTDH method

The MultiConfiguration Time Dependent Hartree (MCTDH)[22–25] is a time-dependent method in which each degree of freedom is associated with a small number of orbitals or single particle functions (SPFs) which, through their time dependence, allow an efficient description of the molecular dynamic process. The total MCTDH wave function is expanded in Hartree products, that is,

products of single-particle functions,

$$\Psi(Q_1, \ldots, Q_f, t) = \sum_{j_1=1}^{n_1} \cdots \sum_{j_f=1}^{n_f} A_{j_1\cdots j_f}(t) \prod_{\kappa=1}^{f} \varphi_{j_\kappa}^{(\kappa)}(Q_\kappa, t)$$
$$= \sum_J A_J \Phi_J, \quad (1)$$

where f is the number of degree of freedom of the system and Q_1, ..., Q_f are the nuclear coordinates. J is a composite index such that

$$A_J \equiv A_{j_1\cdots j_f} \quad \text{and} \quad \Phi_J \equiv \prod_{\kappa=1}^{f} \varphi_{j_\kappa}^{(\kappa)}.$$

$A_{j_1\cdots j_f}$ denotes the MCTDH expansion coefficients, and $\varphi_{j_\kappa}^{(\kappa)}(Q_\kappa, t)$ are the n_κ SPFs associated with each degree of freedom κ. The subsequent equation of motion for the coefficients and single particle functions, obtained by applying the Dirac-Frenkel variational principle to the wave function *ansatz*, are a set of coupled nonlinear differential equations that conserve the norm and the total energy (for time-independent Hamiltonian).

The MCTDH equations of motion are solved at every time step and require to build the *mean fields* and the Hamiltonian matrix. The Hamiltonian matrix and *mean fields* require evaluation of integrals of the type

$$\left\langle \varphi_{j_1}^{(1)} \cdots \varphi_{j_f}^{(f)} | \hat{H} | \varphi_{l_1}^{(1)} \cdots \varphi_{l_f}^{(f)} \right\rangle. \quad (2)$$

Because of the considerable time those calculations take in the process of a computation, the MCTDH approach relies in transforming the Hamiltonian operator $\hat{H}$ to a sum-of-products of single particle operators,

$$\hat{H} = \sum_{r=1}^{s} c_r \prod_{\kappa=1}^{f} \hat{h}_r^{(\kappa)}, \quad (3)$$

which then significantly simplifies the evaluation of the Hamiltonian matrix and the *mean fields*

$$\left\langle \varphi_{j_1}^{(1)} \cdots \varphi_{j_f}^{(f)} | \hat{H} | \varphi_{l_1}^{(1)} \cdots \varphi_{l_f}^{(f)} \right\rangle = \sum_{r=1}^{s} c_r \prod_{\kappa=1}^{f} \left\langle \varphi_{j_\kappa}^{(\kappa)} | \hat{h}_r^{(\kappa)} | \varphi_{l_\kappa}^{(\kappa)} \right\rangle. \quad (4)$$

In Subsections II B and II C, we will describe the expression of the Kinetic Energy Operator and the Potential Energy Operator as a sum-of-products of single particle operators.

B. MCTDH kinetic energy operator

We described quite extensively in the previous paper[26] on this system the Hamiltonian [Kinetic Energy Operator (KEO) and Potential Energy Surface (PES)]. The Kinetic Energy Operator (KEO) expressed in Jacobi coordinates is used in this work, following the subsystem KEO derivation presented by Brocks *et al.*[27] and generalized by Gatti and Iung.[28] Here, just as in our previous work[26] on the same system, we work in the E_2 frame obtained by rotation of the first two Euler angles of the SF frame. Althrough this section, we express the KEO in atomic units.

$$2\hat{T} = -\frac{1}{\mu_R} \frac{\partial^2}{\partial R^2} + 2\hat{T}_1 + 2\hat{T}_2 + \frac{1}{\mu_R R^2} \left(\hat{\vec{J}}^\dagger \hat{\vec{J}} + (\hat{\vec{L}}_1 + \hat{\vec{L}}_2)^2 - 2(\hat{\vec{L}}_1 + \hat{\vec{L}}_2)\hat{\vec{J}} \right)_{E_2}, \quad (5)$$

where in the expression of the KEO a factor R is assumed to be included in the wavefunctions, μ_R is the reduced mass of the H_2O–H_2 cluster, the 1 and 2 subscripts refer respectively to the H_2O and H_2 fragments. The rigid rotor Hamiltonian of the H_2O molecule is expressed as[27,29]

$$\hat{T}_1 = \frac{A}{2}\left(\hat{L}_{1,+}^2 + \hat{L}_{1,-}^2 + \hat{L}_{1,+}\hat{L}_{1,-} + \hat{L}_{1,-}\hat{L}_{1,+}\right)_{BF_1}$$
$$- \frac{C}{2}\left(\hat{L}_{1,+}^2 + \hat{L}_{1,-}^2 - \hat{L}_{1,+}\hat{L}_{1,-} - \hat{L}_{1,-}\hat{L}_{1,+}\right)_{BF_1} + B\hat{L}_{z^{BF_1}}^2, \quad (6)$$

where the rotational constants[10] have values $A = 27.8572 \text{ cm}^{-1}$, $B = 14.5145 \text{ cm}^{-1}$, and $C = 9.2799 \text{ cm}^{-1}$. The rigid rotor kinetic energy of the H_2 fragment is written simply as $\hat{T}_2 = B_{H_2}\hat{L}_2^2$ where the rotational constant $B_{H_2} = 59.2434 \text{ cm}^{-1}$. The final form of the KEO obtained after some analytical development and which is implemented in the MCTDH code is then

$$2\hat{T} = -\frac{1}{\mu_R}\frac{\partial^2}{\partial R^2} + 2\hat{T}_1 + 2\hat{T}_2$$
$$+ \frac{1}{\mu R^2}\left(J(J+1) + \hat{L}_1^2 + \hat{L}_2^2 - 2\hat{L}_{1,z}^2 - 2\hat{L}_{2,z}^2\right)_{E_2}$$
$$+ \frac{1}{\mu R^2}\left(\hat{L}_{1,+}\hat{L}_{2,-} + \hat{L}_{1,-}\hat{L}_{2,+} - 2\hat{L}_{1,z}\hat{L}_{2,z}\right)_{E_2}$$
$$+ \frac{1}{\mu R^2}\left(C_+(J,K)(\hat{L}_{1,+} + \hat{L}_{2,+})\right)_{E_2}$$
$$+ \frac{1}{\mu R^2}\left(C_-(J,K)(\hat{L}_{1,-} + \hat{L}_{2,-})\right)_{E_2}, \quad (7)$$

with

$$C_\pm(J,K) = \sqrt{J(J+1) - K(K \pm 1)}. \quad (8)$$

In the preceding equations, the total angular momentum has been integrated over the Wigner matrix elements D_{MK}^J of the overall rotation, $M = 0$ (the projection of J on z_{SF} is arbitrary), and K is the projection of J on the intermolecular axis z_{BF}. $\hat{\tilde{L}}_X$ ($X = 1, 2$) is the total angular momentum of fragment 1 or 2, and $\hat{L}_{X,\pm}$ are their corresponding creation and lowering operators expressed as $\hat{L}_{X,\pm} = \hat{L}_{X,x} \pm \hat{L}_{X,y}$. In terms of angles, we can write for their expressions in the E_2 frame

$$\hat{L}_1^2 = -\frac{1}{\sin\beta}\frac{\partial}{\partial\beta}\sin\beta\frac{\partial}{\partial\beta} + \frac{k_1}{\sin^2\beta}, \quad (9)$$

$$\hat{L}_2^2 = -\frac{1}{\sin\theta}\frac{\partial}{\partial\theta}\sin\theta\frac{\partial}{\partial\theta} + \frac{k_2}{\sin^2\theta} \quad (10)$$

and

$$\hat{L}_{1\pm} = \pm\frac{\partial}{\partial\beta} - k_1\cot\beta, \quad (11)$$

$$\hat{L}_{2\pm} = \pm\frac{\partial}{\partial\theta} - k_2\cot\theta, \quad (12)$$

with an additional shift $k \to k \pm 1$ in Eqs. (11) and (12) to lower or raise the magnetic quantum number. In the BF_1 frame (for H_2O), we have similar expressions with k_1 changed into m_1 and the corresponding additional shift $m_1 \to m_1 \pm 1$,

$$\hat{L}_1^2 = -\frac{1}{\sin\beta}\frac{\partial}{\partial\beta}\sin\beta\frac{\partial}{\partial\beta} + \frac{m_1}{\sin^2\beta}, \quad (13)$$

and

$$\hat{L}_{1\pm} = \pm\frac{\partial}{\partial\beta} - m_1\cot\beta. \quad (14)$$

C. MCTDH potential energy operator

We use as in our previous work[26] the same PES of Valiron et al.[30] and transform it to the appropriate set of coordinates,[26] but now for scattering calculations. Using the multipolar description of Valiron PES and the transformation suggested by Avoird and Nesbitt,[9] we can have an analytically exact representation of the PES in the set of coordinates used for the dynamics and thus are able to extend the PES to any distance without doing an additional refitting with MCTDH. This analytical representation of the PES is particularly useful as the R coordinate's range can be extended as much as needed to accurately describe the low energy region of the cross section. The surface from Ref. 30 after transformation from its original set of coordinates to the E_2 frame can be expressed as

$$V(R, \beta_1, \gamma_1, \alpha_1, \theta_2, \phi_2) = \sum_{\substack{r_\beta, r_\gamma \\ r_\alpha, r_\theta}} \tilde{V}_{\substack{r_\beta, r_\gamma \\ r_\alpha, r_\theta}}(R) f_{\substack{r_\beta, r_\gamma \\ r_\alpha, r_\theta}}(\omega_1, \omega_2), \quad (15)$$

where

$$f_{\substack{r_\beta, r_\gamma \\ r_\alpha, r_\theta}}(\omega_1, \omega_2) = D_{r_\alpha, r_\gamma}^{(r_\beta)}(\beta_1, \gamma_1, \alpha_1)^\star C_{r_\theta, -r_\alpha}(\theta_2, \phi_2). \quad (16)$$

$D_{r_\alpha, r_\gamma}^{(r_\beta)}(\beta_1, \gamma_1, \alpha_1)$ is the Wigner D-matrix and $C_{r_\theta, -r_\alpha}(\theta_2, \phi_2)$ is the Racah normalized spherical harmonics. As we work in the momentum representation for the degrees of freedom γ, α, and ϕ, we replace γ_1, α_1, and ϕ_1 by their momentum representation m_1, k_1, and k_2 where we dropped the 1 and 2 indices to simplify the notation.

D. Inelastic cross section calculations

The H_2O + H_2 scattering calculations were designed in a similar way as our previous scattering studies,[8,13,31] where we used the MCTDH program: we will repeat those steps here.

(i) First, a wavepacket defining the initial state has to be constructed: it is here (since we are in the rigid rotor approximation) the product of the initial rotational state of H_2O, the initial rotational state of H_2, and a Gaussian function along the dissociative coordinate R, starting far away from the interaction region. The Gaussian's parameters (with a negative impulsion) are selected in order to cover the energy range of interest. The initial wavefunction is thus expressed as

$$\Psi_i(R, \beta, m_1, k_1, \tilde{\theta}, k_2) = \psi_i(\beta, m_1, k_1, \tilde{\theta}, k_2)\chi(R)$$
$$= \tau_{1,i}(\beta, m_1, k_1)\tau_{2,i}(\theta, k_2)\chi(R), \quad (17)$$

where ψ_i is a product of the initial rotation states of H_2O ($\tau_{1,i}$) and H_2 ($\tau_{2,i}$). The initial rotational state of H_2O are linear combination of Wigner-D matrices usually written in the simplified notation $j_1 K_a K_c$, where j_1 is the molecular rotational angular momentum and K_a, K_c the projection on the molecular BF z-axis along the prolate and oblate limits. If, for example, we write the Wigner D-matrices as $|j_1, k_1, m_1\rangle$,

with m_1 as the projection along the molecule BF z-axis and k_1 as the projection along the SF z-axis (which for the dimer is the intermolecular axis), then the rotational state for the asymmetric top is written as $|j_1, k_1, m\rangle$, where

$$|j_1, k_1, m\rangle = \sum_{m=-j_1}^{j_1} c_{m,m_1} |j_1, k_1, m_1\rangle,$$

where $|j_1, k_1, m_1\rangle$ is the Wigner D-matrix and $m = K_a - K_c$ is an index running from $-j_1$ to j_1. For $j_1 = 0$, the rotational state for the asymmetric top is $|0_{00}\rangle = |0, 0, 0\rangle$ with eigenvalue 0. The rotational states for $j_1 = 1$ are[10]

$$|1_{10}, k_1\rangle = \frac{1}{\sqrt{2}}[|1, 1, k_1\rangle + |1, -1, k_1\rangle],$$

$$|1_{11}, k_1\rangle = |1, 0, k_1\rangle,$$

$$|1_{01}, k_1\rangle = \frac{1}{\sqrt{2}}[|1, 1, k_1\rangle - |1, -1, k_1\rangle], \qquad (18)$$

with respective eigenvalues $A + B$, $A + C$, and $B + C$ (clearly with a $2j_1 + 1 = 3$ degeneracy) with A, B, and C being the rotational constants of H_2O given above and $k_1 = -1, 0, 1$ the magnetic quantum number projections. For $j_1 = 2$, we used the symbolic arithmetic program Sympy[32] to obtain the normalized eigenfunctions and related eigenvalues that helped to analytically generate the initial but also the final rotational functions. While it is obviously not compulsory to obtain the initial and final functions analytically, it nevertheless helps to verify that these results match the known analytical results for this rotational Hamiltonian. For any j's, we more generally use a numerical program to generate the eigenvalues and eigenvectors of the asymmetric top and is thus used to build any initial or final rotational function.

The initial state of H_2 is an associated Legendre polynomial that we write simply as j_2k_2, where j_2 is the molecular angular momentum of the H_2 fragment and k_2 the projection along the BF-axis. The Gaussian χ is written as

$$\chi(R) = \frac{1}{\sqrt{2\pi}w} \exp\left[-\left(\frac{R - R_0}{2w}\right)^2\right] e^{ip_0(r - R_0)} \qquad (19)$$

with R_0, p_0, and w being respectively its center in coordinate and momentum space and its width. For this work, we tested various parameters and two sets of energy distributions (for which a state-to-state cross section will be presented later) are shown in Fig. 2.

When the initial rotational states of H_2O or H_2 have a nonzero angular quantum number ($j_1 \neq 0$ in $j_1K_aK_c$ or $j_2 \neq 0$ in j_2k_2), then calculations for each magnetic quantum number projection have to be done also in order to obtain the state-to-state cross-sections from a specific initial rotational state. The lowest *para* and *ortho* rotational levels of H_2O and H_2 are presented in Table I. The parameters were taken to be similar to the ones used for the MOLSCAT calculations which are considered to be exact.[20] Using MOLSCAT, calculations for *para*-H_2 were done with $j_{1,max} = 5$, $j_{2,max} = 2$, and $J_{TOT,max} = 35$. A test of $j_{2,max} = 4$ was done and displayed a change of less than 0.1% in the Time Independent cross

TABLE I. Rotational energy levels (cm^{-1}) or *ortho* and *para* H_2O and H_2. The rotational constants used to generate those levels are $A = 27.8572$ cm^{-1}, $B = 14.5145$ cm^{-1}, and $C = 9.2799$ cm^{-1} for H_2O and $B_{H_2} = 59.2434$ cm^{-1} for H_2. *Ortho* levels of H_2 are displayed in italics.

| | H_2O | | | H_2 | |
	ortho		*para*		*ortho* and *para*
1_{01}	23.7995	0_{00}	0.000 00	0	0.0000
1_{10}	42.4024	1_{11}	37.158 3	*1*	*118.4868*
2_{12}	79.5133	2_{02}	70.132 9	2	355.4604
2_{21}	135.3220	2_{11}	95.245 4	*3*	*710.9208*
3_{12}	173.5976	2_{20}	136.587 6	4	1184.8680

sections. The $2j_1 + 1$ (and $2j_2 + 1$) repetition of the calculations is avoided due to the symmetry of H_2O (and H_2). If we write an initial rotational eigenstate of H_2O as $|j_1, k_1, m_1\rangle$ (H_2 as $|j_2, k_2\rangle$), then the state-to-state probabilities from the initial states $|j_1, k_1, m_1\rangle$ and $|j_1, -k_1, m_1\rangle$ ($|j_2, k_2\rangle$ and $|j_2, -k_2\rangle$) are identical, and instead of running for a rotational state $j_1K_aK_c$ of H_2O and j_2 of H_2 $(2j_1 + 1) \times (2j_2 + 1)$ calculations, we can simply run $(j_1 + 1) \times (j_2 + 1)$ calculations to obtain the cross sections.

(ii) Next, we have to use a suitable Complex Absorbing Potential (CAP). The intensity of the CAP was determined using the program plcap included in the MCTDH package. As before the form of the CAP is $W(x) = \eta|x - x_c|^b\Theta(x - x_c)$, where Θ is the Heaviside step function, x_c the starting point of the CAP was selected such that the length of the CAP is 20 bohrs, η its strength is 4.76×10^{-9}, and b its order is 4.

(iii) We then have to select primitive basis and SPF bases for the calculation. The primitive basis, its range, and the number of the SPFs used for the wavepacket propagation are summarized in Table II. A primitive basis composed of Fast Fourier Transform (FFT) functions for the intermolecular distance R was coupled with a Wigner-DVR[29] and a two dimensional Legendre-K DVR[33] (a two dimensional extended Legendre DVR similar to Corey and Lemoine's[34]) to describe respectively the orientation of the H_2O and the H_2 fragments in the E_2 frame. For these calculations,

TABLE II. Parameters of the primitive basis used for the rovibrational calculations of H_2O–H_2. FFT stands for the Fast Fourier Transform. Wigner stands for the Wigner DVR. KLeg is the K-Legendre DVR. The units for distance and angle are bohrs and radians, respectively.

Coordinate	Primitive basis	Number of points	Range	Size of SPF basis
R	FFT	960	2.0–72.0	10–20
β	Wigner	6	0–5	10–25
m_1	K	11	−5 to 5	
k_1	K	11	−5 to 5	
$\tilde{\theta}$	KLeg	3	0–2	10–12
k_2	K	5	−2 to 2	

the same primitive basis was used for the calculations of both *para* and *ortho* states of H_2O since the symmetry has not been incorporated yet for the Wigner-DVR in MCTDH.

(iv) As we are interested in the low-energy region of the cross sections, we need to propagate the wavepacket for a very long time. In order to control the propagation and the convergence of the calculation, we allowed the wave packet to propagate for a maximum of 200 ps (with the wavefunction printed every 20 fs) or when 99.0% of the wavepacket has been absorbed by the CAP. For higher values of J, the propagations complete very quickly: for example, for $J = 35$, the calculation stops after about 10 ps while for $J = 0$ a complete 200 ps of propagation is needed and still by that time only about 98.5% of the wavepacket has been absorbed by the CAP. Once the propagations are completed, two procedures can be used to obtain the various state-to-state transition probabilities: it is either the flux[25,35,36] approach or the Tannor and Weeks[37] method. We tested both methods, but we will mainly present results from the Tannor and Weeks method as both results were similar. Unless specified otherwise, in the following equations and text, $E = E_{tot}$, that is, the total energy in the collisional process. The kinetic or collision energy will be labelled E_{kin}. Using the Tannor and Weeks method, the state-to-state reaction probabilities are expressed as[37,38]

$$P_{f \leftarrow i}^{J}(E) = |S_{fi}^{J}(E)|^2$$
$$= \frac{1}{4\pi^2 |\Delta_i(E)|^2 |\Delta_j(E)|^2} \left| \int_0^T e^{iEt} C_{fi}(t) dt \right|^2, \quad (20)$$

where S_{fi} is the S-matrix element and C_{fi} is the autocorrelation function obtained in term of the propagated function Ψ_i and the final state function Ψ_f,

$$C_{fi}(t) = \langle \Psi_f | e^{-iHt} | \Psi_i \rangle, \quad (21)$$

where Δ_i and Δ_f are the energy distribution[39,40] of the initial and final wavepackets, respectively. The functions Ψ_i and Ψ_f are expressed as in Eq. (17) where we can rewrite the labelled transition $f \leftarrow i$ as

$$j_1' k_1' m_1', j_2' k_2' \leftarrow j_1 k_1 m_1, j_2 k_2. \quad (22)$$

Here, $j_1(j_1')$ and $j_2(j_2')$ are respectively the orbital angular momentum quantum numbers of the H_2O and H_2 molecule, $k_1(k_1')$ and $m_1(m_1')$ are respectively the projection of $j_1(j_1')$ along the dimer BF z-axis and the projection of $j_1(j_1')$ along the z-axis of the H_2O monomer Body-Fixed frame. $m_1(m_1')$ along with $j_1(j_1')$ identify specific rotational states of H_2O. $k_2(k_2')$ is the dimer z-axis Body-Fixed projection of $j_2(j_2')$ running from $-j_2$ to $j_2(-j_2'$ to $j_2')$. In the literature, $m_1(m_1')$ is often replaced by $K_a K_c$ where K_a and K_c are respectively the projection of the molecular orbital angular momentum along the Body-Fixed (monomer) axis in the prolate and oblate limits.

As mentioned in a previous publication,[8] while the flux and Tannor and Weeks methods lead to similar probabilities, the flux method usually produces a small, but non-negligible flux in an energetically forbidden region (at energies lower than the total energy threshold). This numerical issue can easily be corrected by zeroing the probabilities in the energetically forbidden region when

summing the cross sections [Eq. (23)]. Conversely, the Tannor and Weeks method requires a broad energy distribution of the final wavefunctions (wavefunctions on which the propagated wavefunction is projected) to make the correlation function disappear more quickly. Following the calculation of the state-to-state transition probabilities, a weighted sum (by the $2J + 1$ factor) of these probabilities then produces the inelastic scattering cross section from the relation

$$\sigma_{j_1 m_1 j_2}^{j_1' m_1' j_2'}(E) = \frac{\pi \hbar^2}{2\mu_R (2j_1+1)(2j_2+1)E_{kin}} \sum_{k_1=-j_1}^{j_1} \sum_{k_2=-j_2}^{j_2} \sum_{k_1'=-j_1'}^{j_1'} \sum_{k_2'=-j_2'}^{j_2'} \sum_{J=0}^{J_{max}}$$
$$\times (2J+1) P_{j_1' k_1' m_1', j_2' k_2' \leftarrow j_1 k_1 m_1, j_2 k_2}^{J}(E), \quad (23)$$

where $E_{kin} = E - E_{int} = E - \epsilon_{H_2} - \epsilon_{H_2O}$ with E_{int}, ϵ_{H_2}, and ϵ_{H_2O} as the internal initial energy of the whole system and the initial rotational energies of the H_2 and H_2O fragments, respectively.

III. RESULTS AND DISCUSSION

Before presenting and discussing the results, it is worth pointing out that the purpose of this work was not simply to demonstrate precise agreement between the MCTDH results and those obtained with the Time-Independent Close-Coupling method (if any could be found), but rather to highlight the computational efficiency with which MCTDH makes it possible to accurately obtain the cross section with reasonably limited resources. However, as the following results will show, we were able to obtain overall a good agreement with Close Coupling results. For all of the calculations reported in this work, we used a primitive and single particle functions basis as reported in Table II. Between 1000 and 6000 single particle functions were used to describe the dynamics of the system compared with more than 1 000 000 primitive basis functions that would have been needed overall for a standard wave packet calculation.

A. Convergence of the calculations

The convergence of the MCTDH calculations depends on various parameters: the primitive basis, the SPF basis, the range of the propagation, the intensity of the CAP, and the duration of the propagation. For this work, we used a primitive basis with angular parameters similar to the one used by Scribano *et al.*:[19] the number of DVR points for the radial degree of freedom was selected to be sufficiently dense for the range selected.

1. Convergence: Radial coordinate range

To determine the range of integration, we performed 2 scattering calculations: one going from 2 to 52 bohrs (with 768 radial DVR points) and the other from 2 to 72 bohrs (with 960 radial DVR points), that is, with about the same density of points along the radial coordinate for the 2 calculations, but also the same number of SPF (1000 SPF for these tests). Those 2 calculations were compared with the available close-coupling calculations (considered exact) as depicted in Fig. 1. As expected, extending the grid and displacing the position of the CAP (which however keeps the same length) improves the quality of the results. Also, the contraction of the grid induces a very small blue shift in the position of the resonance structures of the cross section. We computed the transition
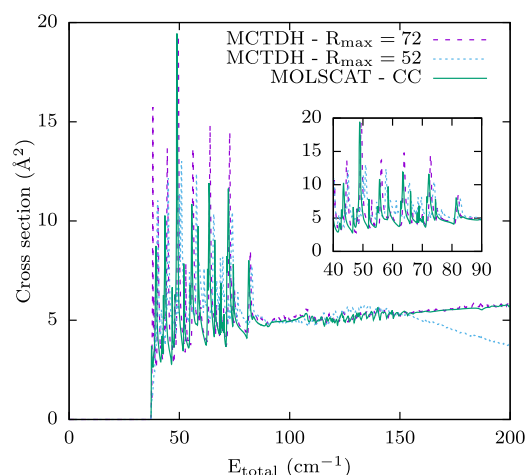
FIG. 1. Comparison of MCTDH calculations for R_{max} = 52 and R_{max} = 72 with time independent close coupling results for the $0_{00} \rightarrow 1_{11}$ rotational transition of H_2O. A zoom of the [40, 90] cm^{-1} is displayed in the inset.

FIG. 2. Energy distribution used for the MCTDH calculations at $J = 0$. edist1 is generated with a Gaussian of width 1.2 a.u. and an initial momentum of -1.6 a.u. and edist2 with a Gaussian of width 1.0 a.u. and a momentum of -2.1 a.u.

probabilities for each individual J from 0 to 35 (the maximum J value considered for the time independent close coupling calculations) in parallel using 32 processors for each J-calculation. These calculations with 1000 SPF lasted from less than a day for the higher J-values to about 7 days for the lower J-values that require a longer propagation. With respect to memory, the calculation for a given J used less than 1Gb of memory to run, but the accumulation of the time dependent wavefunction at each time step can request up to 25 Gb of memory for very long propagations with the largest basis. However, once the probabilities are computed, the wavefunctions are no longer necessary and can be deleted. The duration of these calculations is significantly longer than standard time independent calculations in this energy range. For comparison, single processor MOLSCAT calculations of a single energy point take approximately 1 h. To describe the 0–200 cm^{-1} energy range, 2500 points were computed which is overall 2500 h of CPU time. This amount of CPU time would be on average the time required to compute all the $0_{00} \rightarrow j_{KaKc}$ transitions using the parameters specified earlier. If one is interested in all the cross sections up to $j = 2$ for H_2O, obtaining their cross sections using the approach we presented will be about 22 times more expensive than the CC calculations. Fortunately, several factors may play in favor of the MCTDH implementation. We anticipate, for example, that at higher energies because of the basis increment and the speed of the processes (allowing for a shorter propagation time) the MCTDH calculations for this system and similar ones will become more advantageous than CC calculations.

2. Convergence: The energy distribution

An important aspect of the calculation is the choice of the initial wavefunction. As stated before, the width and initial momentum of the Gaussian are connected to the energy range that will be covered by the scattering calculation. We perform 2 separate scattering calculations to see the influence of the final cross sections on the choice of the energy range covered by the scattering. For the first
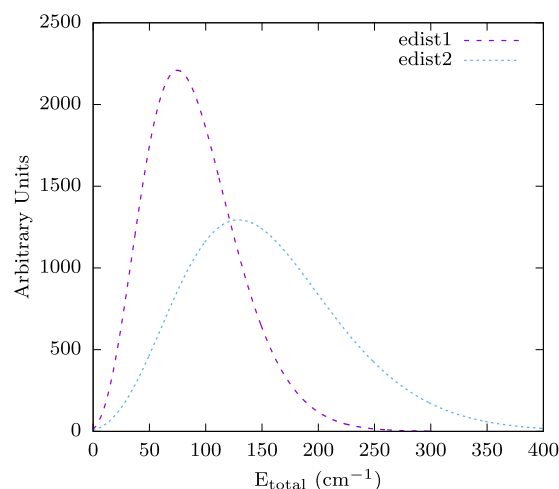
calculation, we selected a Gaussian centered at 52 bohrs with a width of 1.2 a.u. and an initial momentum of -1.6 a.u. (where the negative sign emphasizes the fact that the initial wave packet goes toward the interaction region) and for the second calculation, the Gaussian is centered at 52 bohrs but with a width of 1.0 a.u. and an initial momentum of -2.1 a.u. The energy distributions of the 2 calculations at $J = 0$ are displayed in Fig. 2, and a comparison between the cross sections for the $0_{00} \rightarrow 1_{11}$ transition is compared with the time independent close coupling calculation on Fig. 3. The comparison shows that the calculation with the shorter energy distribution range describes better the low energy than the one with the larger range. Therefore, for calculations spanning a large collisional energy range,
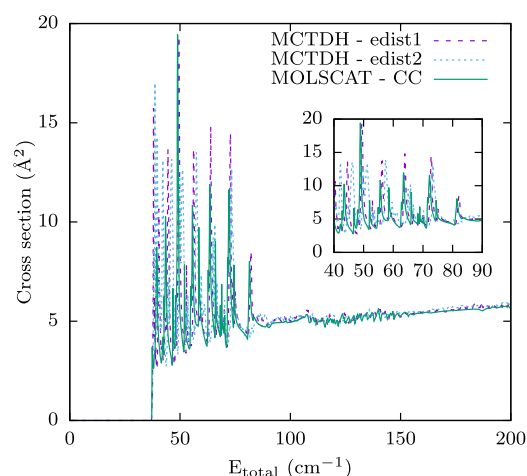

FIG. 3. Comparison of MCTDH calculations for edist1 and edist2 with time independent close coupling results for the $0_{00} \rightarrow 1_{11}$ rotational transition of H_2O. A zoom of the (40, 90) cm^{-1} is displayed in the inset.

it would be necessary to perform different sets of calculations with two or more energy distribution ranges in order to cover accurately a wide range of collision energies.

3. Convergence: The SPF basis

An advantage of the MCTDH method is that the approach, just like the Close Coupling method, is variational. Therefore, we know that once a suitable choice of a primitive basis is made, we can improve the accuracy of the calculation by further increasing the size of the SPF basis. A characteristic of the MCTDH method is that it is designed to reproduce very well the most intense features of a process with a limited number of functions: however, the less intense features can be recovered easily by increasing the size of the SPF basis. In the limit $N_{SPF} \rightarrow N_{PBF}$, we can recover the exact numerically exact calculations, where N_{SPF} and N_{PBF} are the total number of single particle and primitive basis functions, respectively. We were able to verify this feature by looking specifically at the $0_{00} \rightarrow 2_{11}$ transition with an increasing SPF basis, and comparing the results with the exact Time Independent results. One particularity of that transition is that it is about 50 times less intense than the $0_{00} \rightarrow 1_{11}$ transition which is the most intense one and also retrieved from the same set of calculations. We thus selected 4 basis sets which are presented in Table III for the 3 combined modes. During an MCTDH calculation, the SPFs for each mode are arranged according to their weight in the calculation. The parameters mentioned in Table III give the largest combination of SPF basis use for a calculation. However, for calculation at higher J's, the combination of basis numbers that will be used is likely to be smaller. The comparison of the results for the various basis sets is shown in Fig. 4. We can see from the figure that as the SPF basis increases, the agreement with the CC results (which are considered to be exact) improves also significantly.

For the final results reported in this work, we had to decide on convergence criteria. As we had to do several propagations (for each J), and since the SPF basis size decreases as J increases, we chose an SPF basis such that for each (combined) mode, the weight of the last SPF (arranged in decreasing order of weight) should be less than 10^{-5} for all the calculations. This uniform criteria allowed to varying basis which will however maintain a consistent accuracy of the calculation.

B. Rotational excitation cross sections

The calculated inelastic scattering cross sections for the transitions from the ground state to the first excited states, i.e., $0_{00} \rightarrow 1_{11}$, $0_{00} \rightarrow 2_{02}$, and $0_{00} \rightarrow 2_{11}$ are displayed on Figs. 5–7, respectively. The figures show a very good agreement between the MCTDH calculations and the CC calculations at these low energies. In particular, the positions of the resonances are well reproduced in each
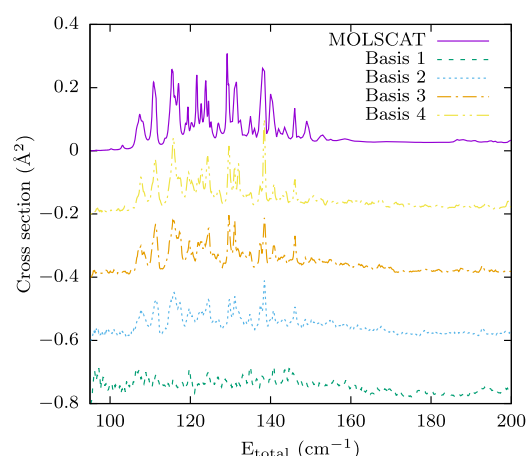

FIG. 4. Comparison between MCTDH calculations for the $0_{00} \rightarrow 2_{11}$ transition with 4 different sets of basis and Exact (MOLSCAT) time independent close coupling calculations. Each MCTDH calculation is shifted by 0.2 Å^2 downward with respect to the previous one, and the most accurate calculation is closer to the MOLSCAT result. The parameters of the basis are given in Table III.

calculation and an even better agreement will certainly be met with a larger SPF basis. The position and the intensity/width of the peaks are connected in the calculations to the range and the duration of the propagation, respectively. A too-narrow range of the propagation shifts the peaks to higher energies because of confinement effects, and a shorter duration of the propagation would make the resonances too broad or even nonexistent. In fact, we actually see in the course of the propagation that some resonances start to appear only after a specific amount of propagation time has elapsed. Similarly, just like with a rovibrational calculation, increasing the size of the (SPF) basis improves the agreement on the peaks position with the time independent calculations, which are considered here to be numerically exact.
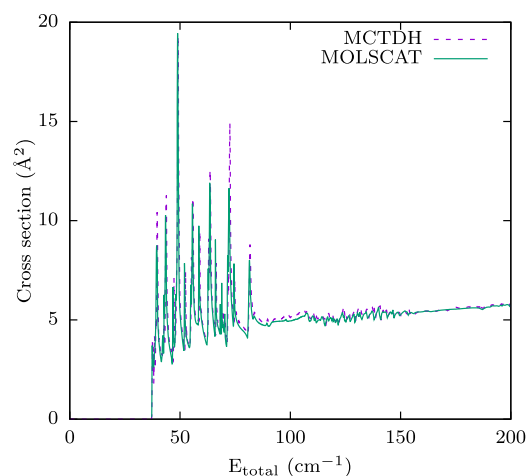

FIG. 5. Comparison of MCTDH calculations with time independent close coupling results for the $0_{00} \rightarrow 1_{11}$ rotational transition of H_2O.
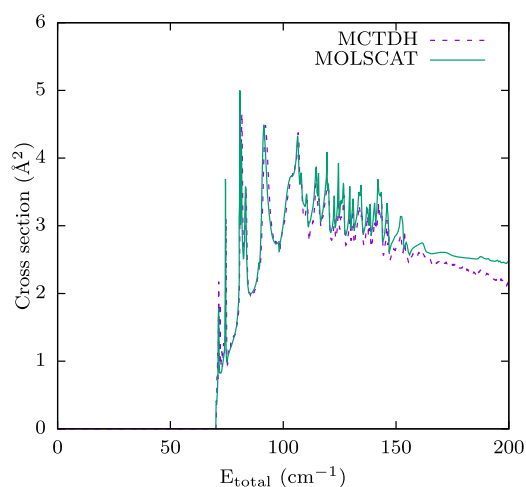
TABLE III. Parameters of the SPF basis used in Fig. 4.

	Basis 1	Basis 2	Basis 3	Basis 4
n_R	10	12	15	20
n_{β, m_1, k_1}	10	15	20	25
$n_{\hat{\theta}, k_2}$	10	10	12	12

FIG. 6. Comparison of MCTDH calculations with time independent close coupling results for the $0_{00} \rightarrow 2_{02}$ rotational transition of H_2O.

FIG. 8. Comparison of MCTDH calculations with time independent close coupling results for the $1_{01} \rightarrow 1_{10}$ rotational transition of H_2O.

Similar to the calculations involving the *para*-states, we performed calculations for the *ortho*-states. Here however, as we mentioned before, we used the same basis sets (made of both *para* and *ortho* rotational states of H_2O) to run the propagation and obtain the cross sections. The excitation cross sections for 2 *ortho* transitions $1_{01} \rightarrow 1_{10}$ and $1_{01} \rightarrow 2_{12}$ are displayed, respectively, in Figs. 8 and 9. Here again, we observe a very good agreement between the MCTDH and the time independent results, both with respect to the position and the intensity of the peaks. We notice however some small issues at the start of the cross sections where some peaks are displayed with a smaller intensity than the time independent results, an issue that is likely linked to the duration of the propagation. Also, toward the high energy side of the spectrum, it appears that the MCTDH calculations have a higher amplitude than the time independent results, an issue that would be corrected if a wider energy
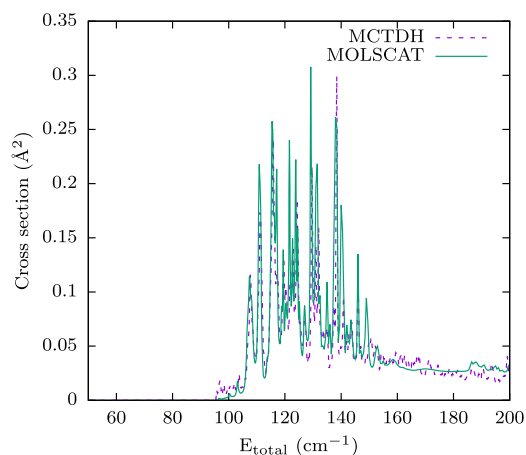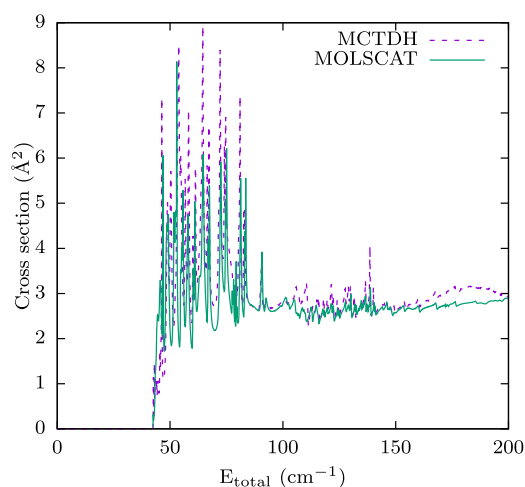
distribution appropriate to describe higher energy values were to be selected.

C. Rotational de-excitation cross sections

We performed additional calculations to determine the state-to-state cross sections from the first excited *para*-state. This allowed us to obtain a de-excitation cross section $1_{11} \rightarrow 0_{00}$ in addition to an excitation cross section $1_{11} \rightarrow 2_{02}$. These cross sections are displayed in Figs. 10 and 11. Note in Fig. 10 the logarithmic scale used for the $y - axis$ (cross section intensity). We observe as in the previous cases that the excitation cross section reproduces quite well the position of the peaks/resonances of the spectrum; this is also the case for the de-excitation process until we get to very low kinetic energy values. However, while the intensities are usually quite well reproduced for
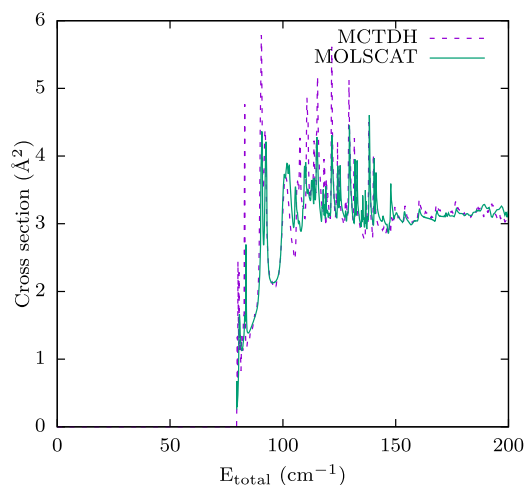

FIG. 7. Comparison of MCTDH calculations with time independent close coupling results for the $0_{00} \rightarrow 2_{11}$ rotational transition of H_2O.

FIG. 9. Comparison of MCTDH calculations with time independent close coupling results for the $1_{01} \rightarrow 2_{12}$ rotational transition of H_2O.
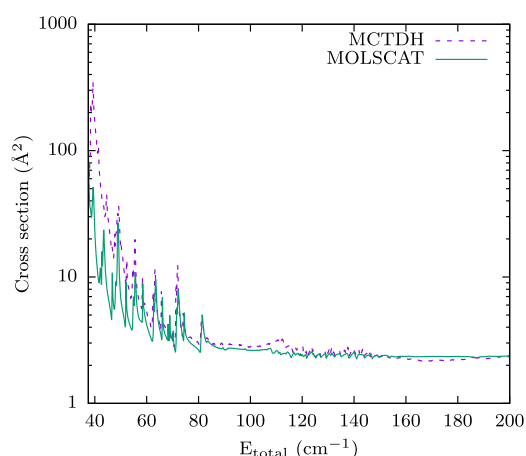
FIG. 10. Comparison of MCTDH calculations with time independent close coupling results for the $1_{11} \rightarrow 0_{00}$ rotational transition of H_2O. Note the logscale applied to the y–axis (cross section intensity).
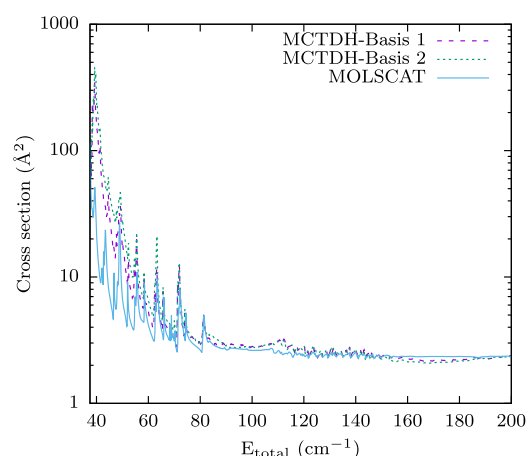

FIG. 12. Comparison of MCTDH calculations—with the smaller (Basis 2) and larger (Basis 1) basis—with time independent close coupling results for the $1_{11} \rightarrow 0_{00}$ rotational transition of H_2O. Note the logscale applied to the y–axis.

the excitation processes, the logarithmic scale cross sections (Fig. 10) highlight how difficult it is to accomplish it for the de-excitation process. This difference in accuracy between the 2 types of calculations (excitation and de-excitation) using the same SPF basis can be understood from the cross sections equation [Eq. (23)] but also from the calculation of state-to-state transition probabilities in the flux formalism. Within this formalism, the transition probabilities are obtained as a ratio of the flux going toward a specific channel to the total flux. When the calculation is exact, the total flux is well approximated by the energy distribution of the propagation. While for the excitation processes the starting point of the state-to-state cross-sections is often in an energy region where the absolute value of the energy distribution is quite significant, for de-excitation processes, this often corresponds to an energy region where the energy

distribution is very small, 2 order of magnitude or more lower than the peak of the energy distribution. As the flux to that channel at low kinetic energy is also very small, it is quite difficult to describe with a small contracted basis designed for the whole energy range, the small features that mainly influence the low kinetic energy domain. Additionally, the $1/E_c$ term amplifies the disagreement between the MCTDH and time independent calculations at low collision energies where its role is alleviated as energy increases as we can see from the picture. However, we realized that by increasing the SPF basis size we were able to significantly improve the comparison with the time independent results. For example, while for most of the calculations displayed in this work we used a SPF basis with parameters described in Table II, and for the $1_{11} \rightarrow 0_{00}$, we used up to 35 SPFs for the H_2O angular basis and up to 25 SPFs for the FFT on the R coordinate
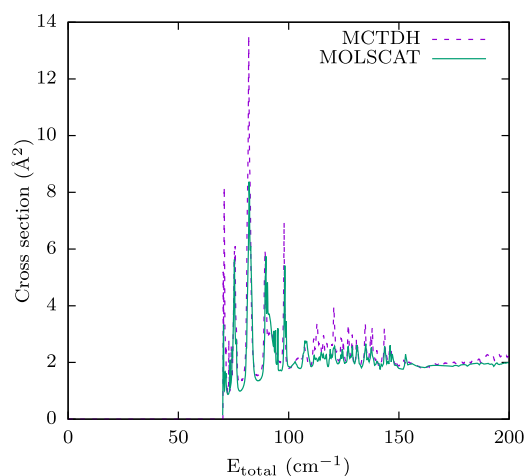

FIG. 11. Comparison of MCTDH calculations with time independent close coupling results for the $1_{11} \rightarrow 2_{02}$ rotational transition of H_2O.
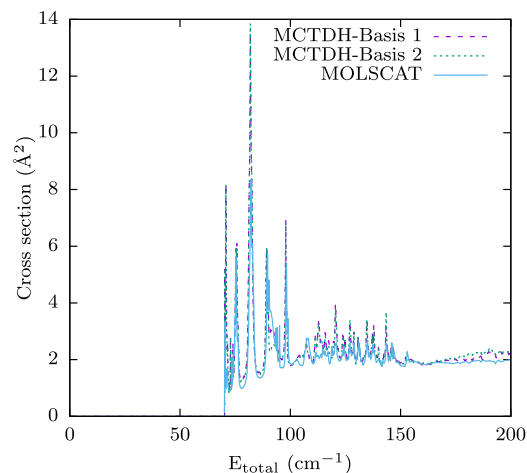

FIG. 13. Comparison of MCTDH calculations—with the smaller (Basis 2) and larger (Basis 1) basis—with time independent close coupling results for the $1_{11} \rightarrow 2_{02}$ rotational transition of H_2O.

on some J propagation that we identified as the most problematic. Despite this significant increase, we noted some (modest) change on the low energy region of the de-excitation cross section for the $1_{11} \rightarrow 0_{00}$ transition while only a modest to nonexistent one on the excitation cross section for the $1_{11} \rightarrow 2_{02}$ transition as we can see on Figs. 12 and 13, respectively. So essentially, we only observe a problem in the de-excitation cross section of the $1_{11} \rightarrow 0_{00}$ transition within 10–20 cm^{-1} above the threshold energy, i.e., here, below ≈ 55 cm^{-1} of total energy E.

IV. CONCLUSION

We performed the first benchmark 5D calculations for the inelastic scattering of an asymmetric top molecule (H_2O) with a linear molecule (H_2), all in the rigid rotor approximation, using the MultiConfiguration Time Dependent Hartree procedure and without any additional approximation on a recently constructed PES. We find as expected a very good agreement between the time independent close coupling results and our calculations which are done however with a significant amount of resources (CPU time) compared to close-coupling calculations.

Time independent close coupling calculations are frequently regarded as the benchmark for these types of atom/molecule or molecule/molecule collisional processes. However, they quickly become intractable when either the density of rotational states of the partners or the dimensionality of the collisional system increases. It then becomes essential to look for alternate means of computing collisional cross sections. We anticipate that the MCTDH procedure (and its variants MultiLayer-MCTDH—ML-MCTDH—, . . .) could be one of those alternate methods to describe fully quantum mechanically the collisional dynamics in these challenging cases. As the MCTDH inelastic scattering calculations usually generate cross sections for all transitions starting from an initial state, they will also be very relevant for comparison with experimental results where quite often only selected transitions could be measured.

With respect to astrophysical applications where one is often interested in the state-to-state rates, instead of the specific state-to-state cross sections, one can infer the state-to-state rate of a de-excitation process (where the cross sections calculations appear to be challenging at low kinetic energy using the MCTDH method) from the reverse excitation process, which is known as detailed balance.

The current MCTDH implementation of the Wigner-DVR does not yet enable even/odd symmetry specified calculations. Hence, it was not possible to selectively perform wavepacket propagation calculations for the *para* and *ortho* cases which have a specific symmetry with respect to the H_2O fragment axis. We thus did not take advantage of the primitive basis size reductions that would occur from the symmetry consideration. As an example, the CPU time will likely be divided by 4, by integrating symmetry in our calculations. Also, a rather conservative maximum time of 200 ps was used for these calculations: it is likely that using 100 or even 50 fs of propagation would generate very similar cross sections. This will then allow us to reduce by about one half or more the cost of our calculations and therefore make them very competitive to close coupling calculations. Nevertheless, we found the calculations for this system still tractable with respect to both the time and memory requirements using our current implementation.

The usage of the MCTDH method for these types of applications is still at a development stage. However, we are working on defining a scheme through which these types of computations would become standard and straightforward for a broader group of people interested in such applications. Imposing the symmetry for the Wigner-DVR in the MCTDH package will be part of this process and will obviously improve the results.

SUPPLEMENTARY MATERIAL

See the supplementary material for a Fortran program and the eigenvalues and eigenvectors of an asymmetric top molecule given the rotational constants A, B, and C.

REFERENCES

[1] A. V. Nesterenok and D. A. Varshalovich, Astron. Lett. **40**, 425 (2014).

[2] M. R. Lerate, J. A. Yates, M. J. Barlow, S. Viti, and B. M. Swinyard, Mon. Not. R. Astron. Soc. **406**, 2445 (2010).

[3] A. Faure and E. Josselin, Astron. Astrophys. **492**, 257 (2008).

[4] F. Daniel, J. Goicoechea, J. Cernicharo, M.-L. Dubernet, and A. Faure, Astron. Astrophys. **547**, A81 (2012).

[5] A. Semenov and D. Babikov, J. Phys. Chem. Lett. **6**, 1854 (2015).

[6] J. Loreau, A. Faure, and F. Lique, J. Chem. Phys. **148**, 244308 (2018).

[7] J. Loreau, F. Lique, and A. Faure, Astrophys. J., Lett. **853**, L5 (2018).

[8] S. Ndengué, R. Dawes, F. Gatti, and H. D. Meyer, Chem. Phys. Lett. **668**, 42 (2017).

[9] A. van der Avoird and D. Nesbitt, J. Chem. Phys. **134**, 044314 (2011).

[10] X.-G. Wang and T. Carrington, Jr., J. Chem. Phys. **134**, 044313 (2011).

[11] Y. Scribano, A. Faure, and D. Lauvergnat, J. Chem. Phys. **136**, 094109 (2012).

[12] Y. Scribano and A. Faure, J. Chem. Phys. **146**, 226102 (2017).

[13] S. A. Ndengué, R. Dawes, F. Gatti, and H. Guo, J. Phys. Chem. A **122**, 6381 (2018).

[14] T. R. Philips, S. Maluendes, and S. Green, J. Chem. Phys. **102**, 6024 (1995).

[15] M. L. Dubernet and A. Grosjean, Astron. Astrophys. **390**, 793 (2002).

[16] A. Grosjean, M. L. Dubernet, and C. Ceccarelli, J. Chem. Phys. **408**, 1197 (2003).

[17] M. L. Dubernet, F. Daniel, A. Grosjean, A. Faure, P. Valiron, M. Wernli, L. Wiesenfeld, C. Rist, J. Noga, and J. Tennyson, Astron. Astrophys. **460**, 323 (2006).

[18] M. L. Dubernet, F. Daniel, A. Grosjean, and C. Y. Lin, Astron. Astrophys. **497**, 911 (2009).

[19] Y. Scribano, A. Faure, and L. Wiesenfeld, J. Chem. Phys. **133**, 231105 (2010).

[20] A. Bergeat, A. Faure, S. B. Morales, A. Moudens, and C. Naulin, J. Phys. Chem. A (2019).

[21] A. Faure, N. Crimier, C. Ceccarelli, P. Valiron, L. Wiesenfeld, and M. L. Dubernet, Astron. Astrophys. **472**, 1029 (2007).

[22] H.-D. Meyer, U. Manthe, and L. S. Cederbaum, Chem. Phys. Lett. **165**, 73 (1990).

[23] U. Manthe, H.-D. Meyer, and L. S. Cederbaum, J. Chem. Phys. **97**, 3199 (1992).

[24] *Multidimensional Quantum Dynamics: MCTDH Theory and Applications*, edited by H. D. Meyer, F. Gatti, and G. A. Worth (Wiley VCH, Weinheim, 2009).

[25] M. H. Beck, A. Jäckle, G. A. Worth, and H. D. Meyer, Phys. Rep. **324**, 1 (2000).

[26] S. Ndengué, Y. Scribano, D. M. Benoit, F. Gatti, and R. Dawes, Chem. Phys. Lett. **715**, 347 (2018).

[27] G. Brocks, A. V. D. Avoird, B. T. Sutcliffe, and J. Tennyson, Mol. Phys. **50**, 1025 (1983).

[28] F. Gatti and C. Iung, Phys. Rep. **484**, 1 (2009).

[29] C. Leforestier, J. Chem. Phys. **101**, 7357 (1994).

[30] P. Valiron, M. Wernli, A. Faure, L. Wiesenfeld, C. Rist, S. Kedzuch, and J. Noga, J. Chem. Phys. **129**, 134306 (2008).

[31] S. A. Ndengué, R. Dawes, and F. Gatti, J. Phys. Chem. A **119**, 7712 (2015).

[32] A. Meurer, C. P. Smith, M. Paprocki, O. Čertík, S. B. Kirpichev, M. Rocklin, A. Kumar, S. Ivanov, J. K. Moore, S. Singh, T. Rathnayake, S. Vig, B. E. Granger, R. P. Muller, F. Bonazzi, H. Gupta, S. Vats, F. Johansson, F. Pedregosa, M. J. Curry, A. R. Terrel, V. Roučka, A. Saboo, I. Fernando, S. Kulal, R. Cimrman, and A. Scopatz, PeerJ Comput. Sci. **3**, e103 (2017).

[33] S. Sukiasyan and H. D. Meyer, J. Chem. Phys. **116**, 10641 (2002).

[34] G. C. Corey and D. Lemoine, J. Chem. Phys. **97**, 4115 (1992).

[35] T. Seideman and W. H. Miller, J. Chem. Phys. **96**, 4412 (1992).

[36] A. Jäckle and H.-D. Meyer, J. Chem. Phys. **105**, 6778 (1996).

[37] D. J. Tannor and D. E. Weeks, J. Chem. Phys. **98**, 3884 (1993).

[38] A. N. Panda, F. Otto, F. Gatti, and H.-D. Meyer, J. Chem. Phys. **127**, 114310 (2007).

[39] F. Gatti, F. Otto, S. Sukiasyan, and H. D. Meyer, J. Chem. Phys. **123**, 174311 (2005).

[40] A. Jäckle and H. D. Meyer, J. Chem. Phys. **109**, 2614 (1998).